Stability and charge transfer levels of extrinsic defects in $LiNbO_3$

Haixuan Xu (徐海譞),[1] Aleksandr Chernatynskiy,[1] Donghwa Lee (이동화),[1] Susan B. Sinnott,[1] Venkatraman Gopalan,[2] Volkmar Dierolf,[3] and Simon R. Phillpot[1,*]

[1]*Department of Materials Science and Engineering, University of Florida, Gainesville, Florida 32611, USA*

[2]*Department of Materials Science and Engineering, Pennsylvania State University, University Park, Pennsylvania 16802, USA*

[3]*Department of Physics, Lehigh University, Bethlehem, Pennsylvania 18015, USA*

(Received 18 June 2010; published 15 November 2010)

The technologically important incorporation of extrinsic defects (Mg^{2+}, Fe^{2+}, Fe^{3+}, Er^{3+}, and Nd^{3+}) in $LiNbO_3$ is investigated using density-functional theory combined with thermodynamic calculations. Defect energies, the charge compensation mechanisms, and charge transfer levels, are determined for congruent and stoichiometric compositions. In general, under congruent (Nb_2O_5-rich) conditions impurities occupy lithium sites, compensated by lithium vacancies. Under stoichiometric (Li_2O-rich) conditions, impurities occupy both lithium and niobium sites. The effects of the concentration of Mg on the dominant defect and site occupancy are analyzed. In addition, the thermal ionization energy and relative defect stability order for Fe^{2+} and Fe^{3+} are evaluated. The charge transfer levels of impurities with regard to the band structure, and their influences on the optical properties of the material are elucidated.

DOI: 10.1103/PhysRevB.82.184109 PACS number(s): 61.72.J−, 71.15.Mb, 71.55.Ak, 61.72.S−

I. INTRODUCTION

Doped $LiNbO_3$ has applications in many technologies, including lasers, optical amplifiers, and integrated optical circuits.[1–4] To achieve the desired functionalities, various dopants are added to the system. For example, Mg is introduced to increase the resistance to photorefractive damage;[5,6] Fe doping is used for holographic storage and beam coupling;[7] and Nd is added for solid-state laser applications.[8–11] In addition, dopant ions have also been employed as probes to investigate the structure of domain walls and defect/domain-wall interactions.[12–14]

To investigate the site selectivity of dopant ions, various experimental techniques, including electron-spin resonance (ESR),[4] electron nuclear double resonance (ENDOR),[15] Mossbauer spectroscopy,[16,17] Rutherford backscattering,[18] x-ray standing wave (XSW) analysis,[19,20] extended x-ray absorption fine structure (EXAFS),[21] and proton-induced x-ray emission (PIXE) (Ref. 22) have been employed. Moreover, several optical and magnetic resonance spectroscopy studies[23–27] have been used to determine the local environments and configurations around the dopant sites. However, a consensus has not been reached regarding the dominant dopant configurations. While some of these studies used congruent $LiNbO_3$ samples grown by the Czochralski method,[28,29] others used stoichiometric $LiNbO_3$ produced through vapor transport equilibration (VTE).[30–32] It is very difficult to compare results between experiments on samples made with different synthesis technique; as a result, the influence of the sample stoichiometry on the site selectivity and distribution is still unclear.

In the present work, the formation energies of several experimentally pertinent dopants (Mg^{2+}, Fe^{2+}, Fe^{3+}, Er^{3+}, and Nd^{3+}) are determined using density-functional theory (DFT). This enables the prediction of the incorporation site preference and the identification of the corresponding charge compensation mechanisms. The influences of the composition and growth conditions on the defect chemistry are assessed based on the thermodynamic analysis at congruent and stoichiometric growth conditions, respectively. Furthermore, the degree of charge transfer of iron with regard to the band structure is calculated to elucidate the effects of coexistence of 2+ and 3+ charged ions on the optical properties of $LiNbO_3$. The possible charge transfer levels caused by intrinsic defects are also considered.

II. METHODOLOGY

A. Density-functional theory calculations

The DFT (Refs. 33 and 34) calculations use the projected augmented wave method[35] combined with the generalized gradient approximation (GGA), as implemented in the Vienna *ab initio* simulation package (VASP).[36,37] The cut-off energy for the plane-wave basis set is chosen to be 400 eV based on convergence tests.[38] The system size is $2\times2\times1$ unit cells (each of 30 atoms), for a total of 120 atoms and 720 valence electrons; periodic boundary conditions are applied in all three dimensions. The integration over the Brillouin zone uses a $4\times4\times2$ Monkhorst-Pack[39] k-point mesh. The structure is optimized to within an error in energy and forces of 0.001 eV and 0.01 eV/Å, respectively. The Li $2s^1$, Nb $4p^64d^45s^1$, and O $2s^22p^4$ are treated as valence electrons.

Mg has an electronic configuration of $[Ne]3s^2$, in which the two s electrons are considered as valence electrons. For iron, the electronic structure is $[Ar]3d^64s^2$, with the $3d$ and $4s$ electrons treated as valence electrons. Nd is a rare-earth element with electronic structure $[Xe]4f^36s^2$. The frozen core approximation[40,41] is used, in which two of the three f electrons are treated as the frozen core in VASP with only a single f electron treated as a valence electron.[42]

In addition, the $6s^2$ and $5p^6$ are also treated as valence electrons, resulting in a total of nine valence electrons. In general, mean-field theories, such as the local-density approximation (LDA) and GGA, cannot accurately describe the strong correlations of d and f electrons.[42–44] Thus, in ad-

TABLE I. Fundamental properties comparison between GGA, GGA+U, and experiments for FeO and Fe_2O_3.

FeO	GGA	GGA+U (4 eV)	GGA+U (6 eV)	Experiment
Crystal structure	$Fm\bar{3}m$	$Fm\bar{3}m$	$Fm\bar{3}m$	$Fm\bar{3}m$ (Ref. 51)
Lattice constants (Å)	4.088	4.382	4.382	4.334 (Ref. 52)
Magnetic moment (μ_B/atom)	1.009	3.755	3.8	4.2 (Ref. 53)
Band gap (eV)	0.0	1.7	2.02	2.4 (Ref. 54)
Fe_2O_3	GGA	GGA+U (4 eV)	GGA+U (6 eV)	Experiment
Crystal structure	$R\bar{3}c$	$R\bar{3}c$	$R\bar{3}c$	$R\bar{3}c$ (Ref. 55)
Lattice constant, a (Å)	4.698	5.02	5.018	5.0355 (Ref. 56)
Lattice constant, c (Å)	13.376	13.716	13.685	13.7471 (Ref. 56)
Magnetic moment (μ_B/atom)	0.734	4.071	4.222	4.9 (Ref. 57)
Band gap (eV)	0.64	2.08	2.76	2.0–2.7 (Ref. 54)

dressing this problem, either high-level theory, such as the GW approximation[45] or a correction to LDA or GGA, such as the DFT+U approach[46,47] is typically required. In this study, DFT+U with Dudarev's approach[46] is used, in which only the difference between U and J is meaningful. To evaluate the effects of +U, several fundamental properties, including lattice constants, band gap, and magnetic moments, are calculated using GGA and GGA+U for the reference binary Nd and Fe oxides and compared with experimental data. Since Mg does not have d or f electrons, no +U correction is necessary.

B. Effect of +U

For iron oxides, there are several studies focusing on the parametrization of the U and J values. In general, different values are appropriate for LDA and GGA calculations. The most widely used value for LDA calculations is $U-J=4$ eV,[48] which is based on the analysis of heat of formation data.[48] As for GGA+U, both $U-J=4$ eV and $U-J=6$ eV have been used in previous studies.[49,50] Since the aim of this section is to evaluate the effects of +U, both values are employed for the GGA studies of FeO and α-Fe_2O_3

The fundamental properties of FeO and Fe_2O_3 are calculated using GGA and GGA+U and compared with experimental data (Table I).[52–57] For FeO, it is found that GGA underestimates the lattice constant by ~0.21 Å and predicts the band structure to be metallic, a well-known failure of this method. In addition, GGA also severely underestimates the magnetic moment, which is only about one quarter of the experimental value. By contrast, GGA+U overestimates the lattice parameter by a modest 0.08 Å and predicts FeO to be a semiconductor; it predicts a band gap of 1.7 eV ($U-J=4$ eV) and 2.02 eV ($U-J=6$ eV), which are both lower than the experimental value of 2.4 eV.[54] For α-Fe_2O_3, the effects of GGA+U are similar. GGA underestimates the lattice constants by 0.338 Å and 0.371 Å in a and c direction, respectively, while GGA+U ($U-J=4$ eV) are merely 0.016 and 0.031 Å smaller than the experimental values. The band gap calculated using GGA is only 0.64 eV, which is significantly lower than experimental band gap of 2.7 eV. The GGA+U ($U-J=6$ eV) calculations predict the band gap to be 2.76 eV, very close to the experimental value. Comparing the +U parameters, the differences in calculated properties using these two parameters is relatively small. In general, $U-J=6$ eV provides slightly better lattice constants, band gap, and magnetic moments. Consequently, this value is used for the defect formation energies (DFEs) calculations below.

The effect of +U for Er has been evaluated and discussed in a previous study.[58] The following parameters were tested: $U-J=10.3$ eV,[59] $U=8.6$ eV, $J=0.75$ eV,[60] and $U-J=4$ eV. The changes caused by the +U in the electronic structure and the defect energetics were found to be insignificant for even the largest value of $U-J$, indicating that Er is reasonably described by GGA without any +U correction.

There are no values for the +U parameters for either Nd_2O_3 or for Nd in $LiNbO_3$ in the literature. For Nd in TiO_2 using LDA+U calculations $U-J=6.5$ eV has been used.[61] Using GGA+U with this value of $U-J$, we calculated the fundamental properties of Nd_2O_3, which has a hexagonal structure. A comparison of fundamental properties of Nd_2O_3 determined from GGA, GGA+U, and from experiments is given in Table II. Unlike the iron oxides, the lattice constants do not depend strongly on the value of U. Both GGA and GGA+U methods underestimate the band gap by ~1.6 eV. This insensitivity to the value of U is similar to what we found to be the case for Er in $LiNbO_3$. Therefore, pure GGA is used for the calculations of the formation energies of Nd-doped $LiNbO_3$.

TABLE II. Properties of Nd_2O_3 from GGA, GGA+U, and experiments.

Nd_2O_3	GGA	GGA+U (6.5 eV)	Experiment
Crystal structure	$P\bar{3}m1$	$P\bar{3}m1$	$P\bar{3}m1$ [a]
Lattice constants, a (Å)	3.839	3.934	3.8827[a]
Lattice constants, c (Å)	5.998	6.107	6.077[a]
Band gap (eV)	4.12	4.24	4.80[b]

[a]Reference 62.
[b]Reference 63.

C. Calculation of defect formation energies

The formation energy of a defect or defects, denoted as α, with charge state q is calculated using the supercell method[64–67]

$$\Delta E_f(\alpha,q,T,P) = E^{total}(\alpha,q) - E^{total}(\text{perfect}) + \sum_i n_i\mu_i - q(\varepsilon_F + E_v + \Delta V), \quad (1)$$

where α is the defect type, q is the charge of the defect(s), T is temperature, and P is the partial pressure of oxygen. $E^{total}(\alpha,q)$ is the total energy obtained from DFT calculation of a supercell with the defect(s); E^{total}(perfect) is the total energy of the supercell without any defects. n_i is the number of ions of species i that have been added to or removed from the supercell when the defects are created; μ_i is the chemical potential of element i. ε_F is the Fermi level with respect to the valence-band maximum (VBM) in the bulk single crystal. E_v is the VBM of the bulk system. ΔV, is the difference in the electrostatic potentials between the defected and undefected systems.[67]

Theoretically, the free energy rather than the total energy should be used in Eq. (1) for the calculation of the DFEs. Since the total internal energy of a supercell calculated with DFT corresponds to the Helmholtz free energy at zero temperature,[68] these calculations neglect the contributions from the vibrational entropy. Fortunately, experimental and theoretical results for entropies of point defects typically fall between 0 to 10k, where k is the Boltzmann constant.[67] Detailed analyses by Kohan *et al.*[69] for ZnO and by He *et al.*[70] for TiO_2 concluded that entropic effects can be neglected. Consequently, the neglect of the entropy term here will not qualitatively change our conclusions.

D. Thermodynamic framework

The chemical potential of each element has to satisfy the constraint that $LiNbO_3$ be stable against decomposition to metallic Li or Nb and to decomposition to the constituent oxides: Li_2O and Nb_2O_5.[71,72] Bringing all of the stability criteria together, we previously constructed the ternary chemical potential map shown in Fig. 1, where the points in chemical-potential space should be analyzed in a manner analogous to that for the composition in a conventional ternary phase diagram.[73] The details of the construction procedure of this map can be found in our previous study,[71] along with a full explanation of each point and line. Two scenarios are most relevant. Under stoichiometric (Li_2O-rich) conditions, the composition-weighted sum of the lithium and oxygen chemical potentials is equal to the total energy of Li_2O, which is line AD in Fig. 1. Similarly, congruent (Nb_2O_5-rich) conditions correspond to the line BC in Fig. 1.

A physical manifestation of Li_2O-rich conditions is the conversion of congruent samples to nearly stoichiometric $LiNbO_3$ using the VTE method, which takes place in a Li_2O vapor.[30–32] In contrast, Nb_2O_5-rich conditions correspond to growth under a Nb_2O_5 vapor and even to the Czochralski process in which congruent $LiNbO_3$ is grown in air. However, based on structural analysis, the local bonding environments of Nb and O in $LiNbO_3$ are similar to that in Nb_2O_5. Therefore, it is assumed here that the congruent melting condition can be analyzed as if it were grown under Nb_2O_5-like conditions.

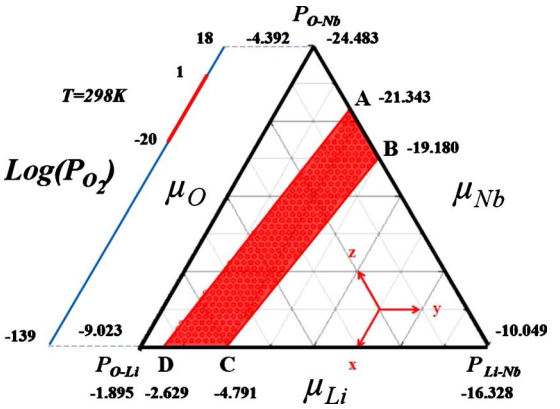

FIG. 1. (Color online) Stability range of chemical potentials (in eV) of the elements in $LiNbO_3$. The region enclosed by points A, D, and $P_{Li\text{-}Nb}$ satisfies the condition that material not decompose into Li_2O while the region enclosed by points B, C, $P_{O\text{-}Li}$, and $P_{O\text{-}Nb}$ satisfies the condition that material not decompose into Nb_2O_5. The intersection of these two regions defines the thermodynamically allowable range of chemical potentials. This stability region is thus defined by the shaded quadrilateral enclosed by the points A, B, C, and D. Line AD represents using Li_2O as reference state; line BC represents using Nb_2O_5 as reference. The oxygen partial pressure range (in atm) is that for room temperature.

The chemical potential of impurities determines *absolute* values for defect energies. Possible choices for the reference state include the pure metal and the binary oxides. Here, the chemical potentials of dopants in $LiNbO_3$ are assumed to be the same as that in binary oxide, which has a very similar bonding environment to that in $LiNbO_3$. For iron oxides, due to the presence of multiple charge states, based on the analysis of the calculated fundamental properties, Fe_2O_3 is chosen to be the reference state. To determine the *relative* stability of these defects, all of the defects structures considered here involve four dopant ions. Thus, the chemical potentials of dopants affect all formation energies equally.

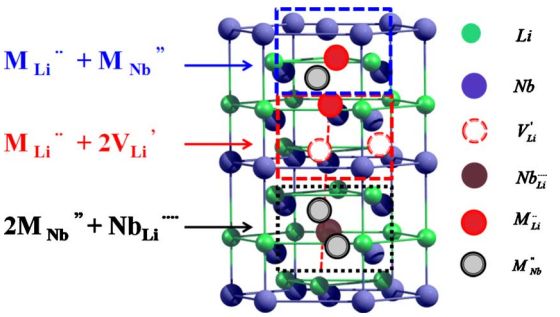

FIG. 2. (Color online) Possible structure of defect cluster consisting of M^{3+} in the system. The oxygen sublattice is not shown.

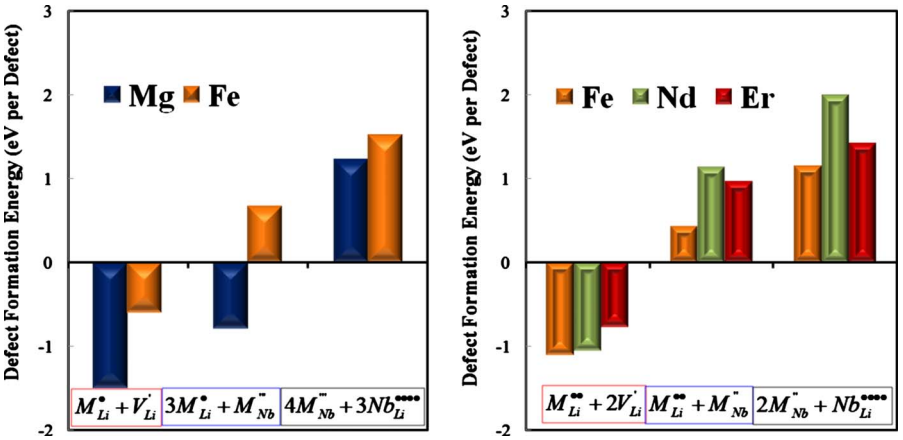

FIG. 3. (Color online) Defect formation energies of various defect reactions for impurities (Mg^{2+}, Fe^{2+}, Fe^{3+}, Nd^{3+}, and Er^{3+}) for the Nb_2O_5 reference state.

III. RESULTS AND DISCUSSIONS

A. Incorporation site preference and charge compensation mechanisms

There are two different charge states of the impurities considered in the current paper: M^{2+} (Mg^{2+} and Fe^{2+}) and M^{3+} (Er^{3+}, Fe^{3+}, and Nd^{3+}). Depending on the charge states, different defect reactions maintain the overall charge balance of the system, resulting in different ratios of the charge compensation species in the system. Based on the previous studies and literature,[74] the following defect clusters are considered in this work: for M^{3+}: (i) $4(M_{Li}^{\cdot\cdot}+2V_{Li}^{'})$, (ii) $2\,(M_{Li}^{\cdot\cdot}+M_{Nb}^{''})$, (iii) $2\,(2M_{Nb}^{''}+Nb_{Li}^{\times\times\times\times})$. for M^{2+}: (i) $4(M_{Li}^{\cdot}+V_{Li}^{'})$, (ii) $3M_{Li}^{\cdot}+M_{Nb}^{''''}$, (iii) $4M_{Nb}^{''''}+3Nb_{Li}^{\times\times\times\times}$.

The possible structures for M^{3+} case are shown in Fig. 2. A summary of the formation energies of these impurities under the Nb_2O_5 reference state is given in Fig. 3. It is noted that under the Nb_2O_5 reference state, the impurities sitting on the lithium site compensated by the lithium vacancies have the lowest formation energies compared with other types of defect clusters. Similar to the intrinsic defects situation, the formation energies are negative, which indicates that the Nb_2O_5 reference state may not accurately represent the experimental growth conditions. However, as the reference state moves from Nb_2O_5 toward Li_2O, there is a range of chemical potential values for which, although the impurities on the lithium site compensated by lithium vacancies have positive DFEs, they are still the lowest and continue to be the dominant defect. The chemical potential within this region is a more accurate representation of the experimental growth environments. The formation energies of impurities given in Fig. 4 are for the Li_2O reference state, which corresponds to the experimental condition of stoichiometric $LiNbO_3$. As the figure shows, all the defects have positive formation energies, leading to very low defect concentrations. This is consistent with the composition being stoichiometric. By comparing different defect clusters, it is found that impurities occupying both lithium and niobium sites have the lowest energy for both M^{2+} and M^{3+}. It is also found that Fe^{3+} is more energetically favorable than Fe^{2+} under both Nb_2O_5 and Li_2O reference states.

It is interesting to examine these results in the context of the experiments. (i) For Mg-doped $LiNbO_3$, the DFT calculations yield the formation energy of the defect cluster with Mg on both lithium and niobium sites as negative, albeit less negative than the defect cluster consisting of Mg on lithium site compensated by lithium vacancies. This indicates there is a strong tendency for Mg to sit on both lithium and niobium sites even under congruent growth conditions, unlike the other impurities considered. Furthermore, the thermodynamic analysis shows that even under Nb_2O_5-rich conditions, the dominant defects may change to Mg on both sites as the chemical potential of Mg increases. The chemical potential can be related with dopant concentration in the usual manner

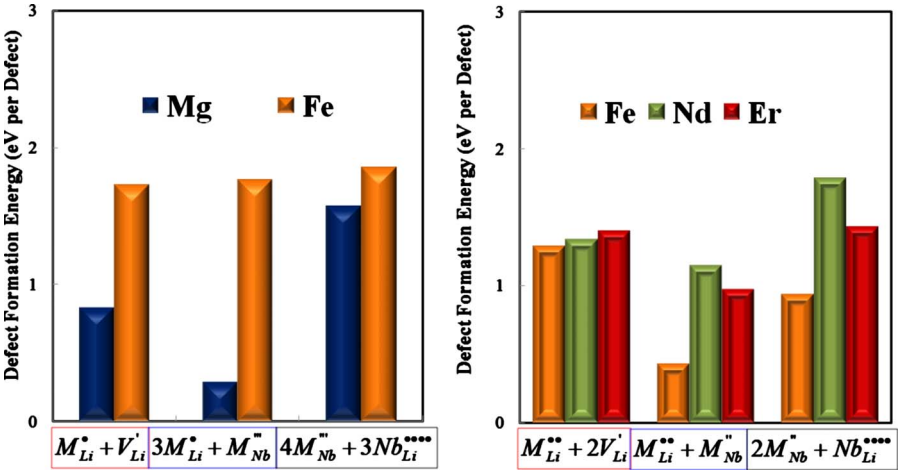

FIG. 4. (Color online) Defect formation energies of various defect reactions for impurities (Mg^{2+}, Fe^{2+}, Fe^{3+}, Nd^{3+}, and Er^{3+}) for the Li_2O reference state.

$$\mu_A = \mu_A^0 + RT \ln X_A \gamma_A, \quad (2)$$

where, μ_A is the chemical potential of the species under the conditions of interest, μ_A^0 is the chemical potential in the standard state, R is the gas constant, T is the temperature, X_A is the concentration, and γ_A is the activity coefficient. Therefore, an increase in the defect concentration will lead to an increase in the chemical potential of the dopant; this will result in a switch of dominant defects from Mg on a lithium site compensated by intrinsic lithium vacancies to Mg on lithium and niobium sites. Experiment has indicated that Mg sits mainly on lithium site at low dopant concentration and on both sites at high concentrations.[5] The DFT predictions are consistent with these experimental observations.

(ii) For Fe-doped $LiNbO_3$, in spite of extensive efforts to determine the occupied site of iron using various techniques, including optical absorption,[75] electron paramagnetic resonance (EPR),[76] Mossbauer spectroscopy,[16,17] and PIXE,[22] no conclusion has yet been reached with regards to site occupancy. ENDOR,[15] PIXE,[22] XSW,[77] and EXAFS (Ref. 78) studies suggest that iron occupies the lithium site. In conflict with these, several studies using EPR and ESR point to iron occupying the niobium site.[76,77] In addition, other studies support a two site model, in which iron occupies both lithium and niobium sites.[79] The DFT calculations find that iron on the lithium site is favorable under both Nb_2O_5- and Li_2O-rich conditions with different charge compensation mechanisms in the two cases. Under the Nb_2O_5 reference state, the intrinsic defects are predicted to be niobium antisites compensated by lithium vacancies. This is consistent with the studies using ENDOR, PIXE, and x-ray-related techniques.[15,22,77] Under Li_2O-rich conditions, which correspond to growth condition of stoichiometric $LiNbO_3$, the compensation mechanism from DFT calculations is predicted to be Fe on a niobium site. However, it is very difficult to observe iron on a niobium site due to existing intrinsic defects.[58] Earlier DFT studies have shown that the presence of even a small concentration of intrinsic defects could make impurities on niobium essentially undetectable. Overall, the DFT calculations indicate that by controlling the experimental conditions or the composition of the material, the site occupancy of the iron can be altered.

Both Fe^{2+} and Fe^{3+} charge states have been considered. In most of the studies, the concentration of iron is very low.[80,81] Furthermore, the concentration of Fe^{2+} is usually at least one order of magnitude lower than Fe^{3+} concentration.[81] Although the concentration ratio of Fe^{2+}/Fe^3 can be varied using thermal treatments or other techniques,[81,82] the naturally occurring concentration ratio of Fe^{2+} and Fe^{3+} indicates that Fe^{3+} is more stable. DFT calculations show that the defect reactions involved with Fe^{3+} have lower formation energies than the reactions that involve Fe^{2+} under all considered reference states, a result that is consistent with the experimental observations.

B. Charge transfer levels of impurities

These Fe^{2+}/Fe^{3+} defects lead to states in the electronic gap. These gap states can be associated with electronic transitions that bring color to materials that are transparent when pure. The location of the charge transfer level is given by[67]

$$E_{\mathrm{PL}} = E_g - E_A - E_{rel}, \quad (3)$$

where E_g is the band gap of the bulk material, E_A is the thermal ionization energy of the acceptor,[67] and E_{rel} is the energy difference associated with the ionic relaxation; this is also called the Franck-Condon shift.[67] The thermal ionization energy, or the energy for removing one electron from the dopant at a particular charge state (such as +2) in $LiNbO_3$, can be calculated from

$$E_A = E_{tot}[M_{\mathrm{Li}}^{\cdot\cdot}] - E_{tot}[M_{\mathrm{Li}}^{\cdot\cdot\cdot}] + E_{corr} - E_v - \Delta V, \quad (4)$$

where $E_{tot}[M_{\mathrm{Li}}^{\cdot\cdot}]$ is the energy of the supercell containing a dopant at a lithium site with +2 charge, $E_{tot}[M_{\mathrm{Li}}^{\cdot\cdot\cdot}]$ is the energy of the supercell containing a dopant at a lithium site with +3 charged; E_{corr} is the energy difference between the highest occupied state and at the special K point and at the Γ point.[67] This correction term is needed because the electrons should be removed from the top of the valence band at the Γ point whereas in DFT the electron is actually taken out of the highest occupied Kohn-Sham level regardless of its k value. E_v is the valence-band maximum of the bulk materials in the calculation, and ΔV is the electrostatic potential difference between the ground-state and photoexcited supercells. The thermal ionization energy of Fe^{2+} in $LiNbO_3$ is calculated to be 1.836 eV, which is consistent with the previous estimates.[83]

The comparison between theoretical calculations and experimental photoluminescence (PL) measurements of Fe-doped $LiNbO_3$ is given in Table III. It is seen that $E_{\mathrm{PL}} \sim 1.4$ eV.[81] The charge transfer level (E_{PL}) of Fe^{2+}/Fe^{3+} is calculated to be 1.34 eV, which is in excellent agreement with the experimental value. However, due to the well-known problem of underestimation of the band gap using DFT, these results have to be treated with caution. This is because the calculated band gap is 0.28 eV lower than the experimental value, which may also be taken to represent the possible error bar of the calculation of the position of the charge transfer level. Using the experimental value of the band gap [3.78 eV (Refs. 87 and 88)], the charge transfer level would be 1.62 eV. There is also error associated with experimental measurements. The experimental photoluminescence measurement below 300 K indicates that the charge transfer level is 1.4 eV.[81] However, after treatment at 520 °C in lithium carbonate, luminescence of an iron center at 1.7 eV was observed.[80] The difference between these experimental observations also indicates the difficulty of determining this value. These experimental and DFT uncertainties notwithstanding, it is worth noting that the DFT calculations lie in the range of both of the experimental values and are consistent with the conjecture that the peak is associated with charge transfer between Fe^{2+} and Fe^{3+}. The relative energy position of Fe^{2+}/Fe^3 with regard to the band gap is given in Fig. 5 with indications of charge transfer level for intrinsic defects $Nb_{\mathrm{Li}}^{4+}/Nb_{\mathrm{Li}}^{5+}$ from DFT calculations. The results of charge transfer level for intrinsic defects $Nb_{\mathrm{Li}}^{4+}/Nb_{\mathrm{Li}}^{5+}$ is consistent with previous first-principles study,[89] predicting it $\sim$0.5 eV below the conduction-band minimum (CBM).

TABLE III. Charge transfer level of impurities calculated by GGA compared with experiments. All the calculations are for impurities on the lithium site.

	Fe^{2+}/Fe^{3+}	Mg^{1+}/Mg^{2+}	Nd^{2+}/Nd^{3+}	Er^{2+}/Er^{3+}	Nb^{4+}/Nb^{5+}
E_A (eV)	1.84	3.42	3.37	2.75	2.76
E_g (eV)	3.50	3.50	3.50	3.50	3.50
E_{rel} (eV)	0.33	0.02	0.01	0.00	0.27
E_{PL} (eV)	1.34	0.06	0.12	0.75	0.47
Experiment (eV)	1.4[a]/1.6[b]	No associated peak[d]	No associated peak[e]	0.80[c]	

[a]Reference 81.
[b]Reference 80.
[c]Reference 84.
[d]Reference 85.
[e]Reference 86.

In the Fe-doped experimental samples with both Fe^{2+} and Fe^{3+} coexisting in the system, the charge transfer level of Fe^{2+}/Fe^{3+} is partially filled. Therefore, the energy needed to excite electrons to the minimum of conduction band is smaller than the band gap. This energy can be provided by incident light in the PL experiments. Once electrons are excited into the conduction band, they may drop to the charge transfer level under the emission of a photon. It is noted that for the system with only Fe^{3+}, the charge transfer level is initially empty. It is possible for an electron to be transferred to the charge transfer level from the valence band. That should produce an absorption peak at about 2.1 eV. Experimentally, the oxygen π orbital to Fe^{3+} was determined to be 3.1 eV above the VBM by Clark *et al.*[90] based on the interpretation of polarized optical absorption spectra. Inconsistent with this, Harhira *et al.*[81] observed the charge transfer level between Fe^{2+} and Fe^{3+} to be 1.4 eV below the CBM from photoluminescence. Although emission and absorption data cannot be directly compared due to configurational relaxation and the formation of polarons, this indicates that there remains experimental uncertainty in the relative position charge transfer level between Fe^{2+} and Fe^{3+} with respect to the band structure of $LiNbO_3$. The charge transfer level proposed here based on the DFT results is consistent with Hahira's work. However, it should be noted that DFT is a ground-state theory while charge transfer is a process involving excited states. The band gap calculated in the present work is 0.28 eV smaller than the experimental value, which represents a potential error associated with these calculations. Nevertheless, the DFT results predict the intervalence transfer between Fe^{2+} and Nb^{5+} is 0.9 eV, which is in agreement with the activation energy for thermal Fe^{2+}-Nb^{5+} electron transfer measured by Clark *et al.*[90] In principle, the charge transfer level of Fe^{2+}/Fe^{3+} might also be observed if the incident light energy is high, as with the band gap energy. In this case, the charge transfer level is initially empty. The electrons are excited from the valance-band maximum to the conduction band. Then the electrons at the conduction band may fall back into the charge transfer level. However, since incident light energies in previous experimental studies are smaller than the band gap, this phenomenon has not been observed.

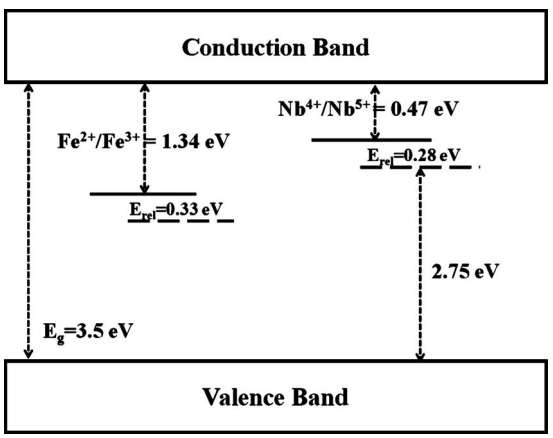

FIG. 5. The position of Fe^{2+}/Fe^{3+} charge transfer level with respect to the band gap.

Using the same approach, the charge transfer levels are calculated for Mg, Nd, and Er. The results of these calculations are given in Table III. The thermal ionization energies for both Mg and Nd are close to the calculated band gap, which result in the E_{PL} being very small. These small values of E_{PL} correspond to very long wavelengths (>10 μm) and the energies are comparably to phonons. Hence no radiative transitions can be observed.

The charge transfer levels in Er are a particularly interesting case. The calculated value of E_{PL} is 0.75 eV, which is pleasingly close to an experimental peak at 0.80 eV (1540 nm).[84,91] However, the theoretical calculation and experiments seem to describe different processes. The experimental peak at 1540 nm is due to a $4f$ to $4f$ transitions within the Er^{3+} ion itself. It has been concluded to be the transition from $^4I_{15/2}$ atomic state of the Er atom to the ground state $^4I_{13/2}$.[84] Such an intrinsic electronic transition is possible due to the shielding of the f shell by electrons located on the outer spherically symmetric s and p shells of the Er atom; this transition does not involve any charge transfer. On the other hand, the calculated E_{PL} simulates a process in which electrons at the conduction-band jump into the charge transfer level. For this process to happen, it is necessary that there be electrons in the conduction band. For Fe doping, there are both Fe^{2+} and Fe^{3+} in the material;[80,81] therefore, there are electrons at the charge transfer level, which is relatively

close to the conduction band and can be excited easily.

There is no Er^{2+} in the system. Thus, the incident light has to photoexcite electrons from the valence to the conduction band. However, the experimental incident light usually has a wavelength longer than 440 nm,[81,84] which is smaller than the band gap. Thus, the charge transfer level cannot be observed from experiments.

IV. CONCLUSIONS

The incorporation site preference and corresponding charge compensation mechanisms of several impurities in $LiNbO_3$ have been predicted based on DFT calculations of possible defect clusters at both congruent and stoichiometric growth conditions. In general, it was found that all the impurities occupy lithium sites compensated by lithium vacancies for the Nb_2O_5 reference state. Impurities on both lithium and niobium sites are predicted to be dominant for the Li_2O reference state. However, due to the effects of intrinsic defects and the method of incorporation impurities, the concentration of impurities on niobium site was predicted to be negligible for stoichiometric sample.

Interestingly, Mg was found to have a strong tendency to occupy both lithium and niobium sites even under Nb_2O_5-rich conditions. Increasing the concentration of Mg will lead to an increase in the value of its chemical potential, which should result in a switch of dominant defects from Mg on a lithium site compensated by intrinsic lithium vacancies, to Mg on both sites. This analysis is consistent with the experimental observation that Mg is mainly on lithium site at low dopant concentration and on both sites at high concentrations. It was also found that Fe^{3+} is more energetically favorable than Fe^{2+} under both reference states. Therefore, without special treatment, Fe^{3+} is predicted to be the majority species. Consistent with this, the concentration of Fe^{2+} is usually at least one order of magnitude lower than Fe^{3+} concentration.

The thermal ionization energies and charge transfer levels of impurities were calculated. The charge transfer level of Fe^{2+}/Fe^{3+} was calculated to be 1.34 eV, which is consistent with the long-standing conjecture that there is charge transfer in Fe-doped $LiNbO_3$. The relative position of this charge transfer level with regard to the band structure was illustrated with consideration of the effects of intrinsic defects $Nb_{Li}^{4+}/Nb_{Li}^{5+}$. The charge transfer level of Mg, Nd, and Er was also calculated and discussed.

ACKNOWLEDGMENTS

This work is supported by the National Science Foundation under Grants No. DMR-0602986 and No. DMR-0303279. The computational resources are provided by the high performance center (HPC) at University of Florida and Florida Laboratory for Advanced Materials Engineering Simulation (FLAMES).

*Corresponding author; sphil@mse.ufl.edu

[1] S. Balsamo, S. Maio, I. Montrosset, H. Suche, and W. Sohler, Opt. Quantum Electron. **31**, 29 (1999).
[2] I. Baumann, S. Bosso, R. Brinkmann, R. Corsini, M. Dinand, A. Greiner, K. Schafer, J. Sochtig, W. Sohler, H. Suche, and R. Wessel, IEEE J. Sel. Top. Quantum Electron. **2**, 355 (1996).
[3] J. Amin, J. A. Aust, D. L. Veasey, and N. A. Sanford, Electron. Lett. **34**, 456 (1998).
[4] V. Voinot, R. Ferriere, and J. P. Goedgebuer, Electron. Lett. **34**, 549 (1998).
[5] R. Mouras, M. D. Fontana, P. Bourson, and A. V. Postnikov, J. Phys.: Condens. Matter **12**, 5053 (2000).
[6] D. A. Bryan, R. Gerson, and H. E. Tomaschke, Appl. Phys. Lett. **44**, 847 (1984).
[7] D. L. Staebler and W. Phillips, Appl. Opt. **13**, 788 (1974).
[8] E. Lallier, Appl. Opt. **31**, 5276 (1992).
[9] E. Lallier, J. P. Pocholle, M. Papuchon, C. Grezesbesset, E. Pelletier, M. Demicheli, M. J. Li, Q. He, and D. B. Ostrowsky, Electron. Lett. **25**, 1491 (1989).
[10] L. F. Johnson and A. A. Ballman, J. Appl. Phys. **40**, 297 (1969).
[11] S. J. Field, D. C. Hanna, D. P. Shepherd, A. C. Tropper, P. J. Chandler, P. D. Townsend, and L. Zhang, Opt. Lett. **16**, 481 (1991).
[12] V. Dierolf, T. Morgus, C. Sandmann, E. Cantelar, F. Cusso, P. Capek, J. Spirkova, K. Polgar, W. Sohler, and A. Ostendorf, Radiat. Eff. Defects Solids **158**, 263 (2003).
[13] V. Dierolf, C. Sandmann, S. Kim, V. Gopalan, and K. Polgar, J. Appl. Phys. **93**, 2295 (2003).
[14] V. Dierolf, C. Sandmann, V. Gopalan, S. Kim, and K. Polgar, Radiat. Eff. Defects Solids **158**, 247 (2003).
[15] H. Sothe and J. M. Spaeth, J. Phys.: Condens. Matter **4**, 9901 (1992).
[16] W. Keune, S. K. Date, I. Dezsi, and U. Gonser, J. Appl. Phys. **46**, 3914 (1975).
[17] W. Keune, S. K. Date, U. Gonser, and H. Bunzel, Ferroelectrics **13**, 443 (1976).
[18] L. Kovacs, L. Rebouta, J. C. Soares, M. F. Dasilva, M. Hageali, J. P. Stoquert, P. Siffert, C. Zaldo, Z. Szaller, and K. Polgar, Mater. Sci. Eng., B **9**, 505 (1991).
[19] T. Gog, M. Griebenow, and G. Materlik, Phys. Lett. A **181**, 417 (1993).
[20] T. Gog, T. Harasimowicz, B. N. Dev, and G. Materlik, Europhys. Lett. **25**, 253 (1994).
[21] C. Prieto and C. Zaldo, Solid State Commun. **83**, 819 (1992).
[22] L. Rebouta, M. F. Dasilva, J. C. Soares, M. Hageali, J. P. Stoquert, P. Siffert, J. A. Sanzgarcia, E. Dieguez, and F. Agullolopez, Europhys. Lett. **14**, 557 (1991).
[23] I. Baumann, R. Brinkmann, M. Dinand, W. Sohler, L. Beckers, C. Buchal, M. Fleuster, H. Holzbrecher, H. Paulus, K. H. Muller, T. Gog, G. Materlik, O. Witte, H. Stolz, and W. von der Osten, Appl. Phys. A: Mater. Sci. Process. **64**, 33 (1997).
[24] T. Nolte, T. Pawlik, and J. M. Spaeth, Solid State Commun. **104**, 535 (1997).
[25] D. M. Gill, J. C. Wright, and L. Mccaughan, Appl. Phys. Lett.

64, 2483 (1994).
[26] D. M. Gill, L. McCaughan, and J. C. Wright, Phys. Rev. B **53**, 2334 (1996).
[27] O. Witte, H. Stolz, and W. vonderOsten, J. Phys. D **29**, 561 (1996).
[28] S. Erdei and V. T. Gabrieljan, Cryst. Res. Technol. **24**, 987 (1989).
[29] H. L. Wang, Y. Hang, J. Xu, L. H. Zhang, S. N. Zhu, and Y. Y. Zhu, Mater. Lett. **58**, 3119 (2004).
[30] F. S. Chen, J. Appl. Phys. **40**, 3389 (1969).
[31] R. L. Holman, *Processing of Crystalline Ceramics* (Plenum, New York, 1978).
[32] R. J. Holmes and D. M. Smyth, J. Appl. Phys. **55**, 3531 (1984).
[33] P. Hohenberg and W. Kohn, Phys. Rev. **136**, B864 (1964).
[34] W. Kohn and L. J. Sham, Phys. Rev. **140**, A1133 (1965).
[35] P. E. Blöchl, Phys. Rev. B **50**, 17953 (1994).
[36] G. Kresse and J. Furthmuller, Comput. Mater. Sci. **6**, 15 (1996).
[37] G. Kresse and J. Furthmuller, Phys. Rev. B **54**, 11169 (1996).
[38] Q. K. Li, B. Wang, C. H. Woo, H. Wang, and R. Wang, J. Phys. Chem. Solids **68**, 1336 (2007).
[39] H. J. Monkhorst and J. D. Pack, Phys. Rev. B **13**, 5188 (1976).
[40] U. von Barth and C. D. Gelatt, Phys. Rev. B **21**, 2222 (1980).
[41] A. Kiejna, G. Kresse, J. Rogal, A. De Sarkar, K. Reuter, and M. Scheffler, Phys. Rev. B **73**, 035404 (2006).
[42] J. Hafner, J. Comput. Chem. **29**, 2044 (2008).
[43] T. Oguchi, K. Terakura, and A. R. Williams, Phys. Rev. B **28**, 6443 (1983).
[44] M. Cococcioni and S. de Gironcoli, Phys. Rev. B **71**, 035105 (2005).
[45] R. M. Martin, *Electronic Structure: Basic Theory and Practical Methods* (Cambridge University Press, Cambridge, UK, 2004).
[46] S. L. Dudarev, G. A. Botton, S. Y. Savrasov, C. J. Humphreys, and A. P. Sutton, Phys. Rev. B **57**, 1505 (1998).
[47] A. I. Liechtenstein, V. I. Anisimov, and J. Zaanen, Phys. Rev. B **52**, R5467 (1995).
[48] L. Wang, T. Maxisch, and G. Ceder, Phys. Rev. B **73**, 195107 (2006).
[49] R. Grau-Crespo, F. Cora, A. A. Sokol, N. H. de Leeuw, and C. R. A. Catlow, Phys. Rev. B **73**, 035116 (2006).
[50] A. Rohrbach, J. Hafner, and G. Kresse, Phys. Rev. B **70**, 125426 (2004).
[51] M. W. Barsoum, *Fundamentals of Ceramics* (Taylor & Francis, Bodmin, Cornwall, UK, 2002).
[52] C. A. McCammon and L. G. Liu, Phys. Chem. Miner. **10**, 106 (1984).
[53] P. D. Battle and A. K. Cheetham, J. Phys. C **12**, 337 (1979).
[54] R. Zimmermann, P. Steiner, R. Claessen, F. Reinert, S. Hufner, P. Blaha, and P. Dufek, J. Phys.: Condens. Matter **11**, 1657 (1999).
[55] C. N. R. Rao and B. Raveau, *Transition Metal Oxides* (Wiley-VCH, New York, 1995).
[56] E. N. Maslen, V. A. Streltsov, N. R. Streltsova, and N. Ishizawa, Acta Crystallogr., Sect. B: Struct. Sci. **50**, 435 (1994).
[57] G. Rollmann, A. Rohrbach, P. Entel, and J. Hafner, Phys. Rev. B **69**, 165107 (2004).
[58] H. X. Xu, D. Lee, S. B. Sinnott, V. Gopalan, V. Dierolf, and S. R. Phillpot, Phys. Rev. B **80**, 144104 (2009).
[59] B. Hourahine, S. Sanna, B. Aradi, C. Köhler, and T. Frauenheim, Physica B **376-377**, 512 (2006).
[60] A. Lazreg, Z. Dridi, F. Benkabou, and B. Bouhafs, Physica B **403**, 2702 (2008).
[61] Y. Wang and D. J. Doren, Solid State Commun. **136**, 186 (2005).
[62] M. Faucher, J. Pannetier, Y. Charreire, and P. Caro, Acta Crystallogr., Sect. B: Struct. Sci. **38**, 344 (1982).
[63] S. Kimura, F. Arai, and M. Ikezawa, J. Phys. Soc. Jpn. **69**, 3451 (2000).
[64] C. G. Van de Walle, P. J. H. Denteneer, Y. Baryam, and S. T. Pantelides, Phys. Rev. B **39**, 10791 (1989).
[65] S. G. Louie, M. Schluter, J. R. Chelikowsky, and M. L. Cohen, Phys. Rev. B **13**, 1654 (1976).
[66] W. E. Pickett, K. M. Ho, and M. L. Cohen, Phys. Rev. B **19**, 1734 (1979).
[67] C. G. Van de Walle and J. Neugebauer, J. Appl. Phys. **95**, 3851 (2004).
[68] K. Reuter and M. Scheffler, Phys. Rev. B **65**, 035406 (2001).
[69] A. F. Kohan, G. Ceder, D. Morgan, and C. G. Van de Walle, Phys. Rev. B **61**, 15019 (2000).
[70] J. He, R. K. Behera, M. W. Finnis, X. Li, E. C. Dickey, S. R. Phillpot, and S. B. Sinnott, Acta Mater. **55**, 4325 (2007).
[71] H. X. Xu, D. Lee, J. He, S. B. Sinnott, V. Gopalan, V. Dierolf, and S. R. Phillpot, Phys. Rev. B **78**, 174103 (2008).
[72] H. X. Xu, D. Lee, S. B. Sinnott, V. Dierolf, V. Gopalan, and S. R. Phillpot, J. Phys.: Condens. Matter **22**, 135002 (2010).
[73] R. DeHoff, *Thermodynamics in Materials Science* (Taylor & Francis, Boca Raton, FL, 2006).
[74] R. M. Araujo, K. Lengyel, R. A. Jackson, L. Kovacs, and M. E. G. Valerio, J. Phys.: Condens. Matter **19**, 046211 (2007).
[75] G. I. Malovichko, V. G. Grachev, and O. F. Schirmer, Solid State Commun. **89**, 195 (1994).
[76] H. Wang, X. Y. Kuang, D. Dong, Y. Xiong, and K. W. Zhou, Physica B **367**, 53 (2005).
[77] T. Gog, P. Schotters, J. Falta, G. Materlik, and M. Grodzicki, J. Phys.: Condens. Matter **7**, 6971 (1995).
[78] D. S. Yang, N. Sung, and T. H. Yeom, J. Phys. Soc. Jpn. **78**, 114605 (2009).
[79] G. I. Malovichko, V. G. Grachev, O. F. Schirmer, and B. Faust, J. Phys.: Condens. Matter **5**, 3971 (1993).
[80] F. Jermann and J. Otten, J. Opt. Soc. Am. B **10**, 2085 (1993).
[81] A. Harhira, L. Guilbert, P. Bourson, and H. Rinnert, Appl. Phys. B: Lasers Opt. **92**, 555 (2008).
[82] G. E. Peterson, A. M. Glass, and T. J. Negran, Appl. Phys. Lett. **19**, 130 (1971).
[83] M. Carrascosa and F. Agullolopez, J. Opt. Soc. Am. B **7**, 2317 (1990).
[84] L. S. Qiang, H. X. Zhang, and C. Q. Xu, Mater. Chem. Phys. **77**, 6 (2003).
[85] I. W. Kim, S. S. Yi, V. F. Pichugin, V. Y. Yakovlev, and M. S. Dmitriev, J. Cryst. Growth **253**, 319 (2003).
[86] J. E. Alfonso, M. J. Martin, and C. Zaldo, Appl. Phys. Lett. **71**, 2904 (1997).
[87] D. Redfield and W. J. Burke, J. Appl. Phys. **45**, 4566 (1974).
[88] A. Dhar and A. Mansingh, J. Appl. Phys. **68**, 5804 (1990).
[89] H. H. Nahm and C. H. Park, Phys. Rev. B **78**, 184108 (2008).
[90] M. G. Clark, F. J. Disalvo, A. M. Glass, and G. E. Peterson, J. Chem. Phys. **59**, 6209 (1973).
[91] D. L. Zhang, D. C. Wang, and E. Y. B. Pun, J. Appl. Phys. **97**, 103524 (2005).